Proc. of Int. Conf. on Advances in Robotic, Mechanical Engg. and Design, ARMED

Parametric Study of Material Removal Rate in SINKING–Electro Chemical Spark Machining Process

Mohan Charan Panda
[1]Department of Mechanical Engineering, GIET, Bhubaneswar, Odisha, India
Email: mohancharan_panda@yahoo.co.in

***Abstract*—The Sinking–Electro Chemical Spark Machining (S–ECSM) process has been successfully applied for cavity machining in electrically non-conducting materials such as glass, quartz, ceramics and composites using non-rotating tool electrode. In the present work, an axisymmetric FEM based transient thermal model has been developed to estimate the temperature distribution within the heat affected zone of single spark in the work piece accounting temperature dependent properties of workpiece and same is used for the determination of material removal rate (MRR) during Sinking–ECSM. The present model is also used to study the influence of different input parameters such as energy partition, duty factor, spark radius and electrolyte concentration on MRR during Sinking–ECSM of silicon nitride workpiece material.**

***Index Terms*— Hybrid machining, MRR, Sinking ECSM, FEM.**

I. INTRODUCTION

Electrically non-conducting advanced ceramic materials, glass, quartz, composites, etc. are gaining industrial acceptance, mainly due to the way in which technological limitations can be overcome by the use of these non-metallic materials. But manufacturing engineers are facing new challenges to shape and size these electrically non-conducting materials economically and efficiently. Machining of these materials by conventional methods is a serious problem yet to be resolved. Ultrasonic Machining (USM), Abrasive Jet Machining (AJM), Laser Beam Machining (LBM), and Electron Beam Machining (EBM) are some of the advanced machining processes that can be used for machining these materials, but surface quality and dimensional accuracy of the machined surfaces are the major concern. The development of the Electro-Chemical Spark Machining (ECSM) is the outcome of machining requirements of such materials.

ECSM is one of the hybrid machining processes (HMPs), combining the features of ECM and EDM, used for machining non-conducting materials. ECSM has been found to machine features in four different ways such as Sinking–ECSM, Drilling–ECSM, Wire Cutting–ECSM and Contour Milling–ECSM. Sinking–ECSM operation usually involves machining of cavity using non-rotating tool electrode where as in Drilling–ECSM a rotating tool electrode is used with the main focus on surface quality of side wall of the hole. Wire Cutting–ECSM is capable to do slicing large volume and complex shape to non-conducting material without the need of full form tool electrode. In Contour Milling–ECSM, a simple shape tool electrode is used to produce 3-D cavity by adapting a movement strategy similar to conventional milling.

Grenze ID: 02.ARMED.2018.7.502

ECSM based on electro-chemical discharge (ECD) phenomena, was presented for the first time in 1968 by Kurafuji as "electrochemical discharge drilling" for micro holes in glass (Kurafuji and Suda, 1968). This process is also referred as Electrochemical Arc Machining (ECAM), Electrochemical Discharge Machining (ECDM), and Spark Assisted Chemical Engraving (SACE) (Wuthrich and Fascio, 2005). Machining with ECD is a complex process influenced by several parameters. Until today it is not yet clear which parameters control mainly the machining.

Bhattacharyya et al. (1999) studied the machining of aluminium oxide (Al_2O_3) ceramic using Sinking–ECSM under varying process parametric conditions such as applied voltage and electrolyte concentration. Sarkar et al. (2006) developed a second order, non-linear mathematical model for determination of MRR, radial overcut (ROC), and thickness of heat affected zone (HAZ), as a function of input parameters such as applied voltage, electrolyte concentration and inter-electrode gap, during Sinking–ECSM operation on silicon nitride. Tandon et al. (1990) carried out experimental study of Sinking–ECSM on Kevlar-fiber-epoxy and glass-fiber-epoxy composites to find the effect of change in voltage and specific conductance of the electrolyte on the MRR, TWR and ROC. Tokura et al. [42] reported "pit forming" by electro-chemical discharge process in non conductive ceramics such as alumina silicon nitride (ASN), alumina, and magnesia silicon nitride (MSN), while using a 0.5 mm diameter Ni needle as tool, 20% NaOH aqueous solution as electrolyte, and 70 V as supply voltage. Chikamori [44] carried out grooving on silicon nitride ceramic with arc discharge in electrolyte. The depth of groove obtained at 165 V in 60 min of machining time was about 1.5 mm while using aqueous solution of $NaNO_3$ as electrolyte.

Gautam and Jain (1998) carried out experiments with the different tool kinematics in electro-chemical spark drilling (ECSD) to enhance the process capabilities. They also carried out the parametric study for observing the effect of tool rotational speed, depth of cut and tool eccentricity on MRR and Material Surface Quality (MSQ). Jain and Adhikary [47] applied ECSM process for cutting of quartz using a controlled feed and a wedge edged tool. In their experiment both cathode and anode have been used as a tool, i.e. ECSM with reverse polarity (ECSMWRP) as well as ECSM with direct polarity (ECSMWDP) have been used to machine quartz plates. They found that the penetration rate as well as kerf width increases with increase in voltage for both reverse and straight polarities, because of high discharge energy for sparking and high rate of chemical reaction at high voltage which results in higher material removal.

Basak and Ghosh (1997) have developed an analytical model for the estimation of MRR, but the basic theory of spark generation proposed by them does not match with the actual situation. Jain et al. (1999) computed material removal rate during Sinking–ECSM using Finite Element Method (FEM). In their model random number generation scheme to locate the spark over the workpiece has been used. They assumed the nature of the spark as prismatic column with square cross-section, which is far from real situation. Bhondwe et al. (2006) developed a FEM model for computation of MRR from two types of material, soda lime glass and alumina during Sinking–ECSM.

From the above literature survey, it can be concluded that very little effort has been made towards modeling of Sinking–ECSM process. Most of the work on this process is experimental and consists of the study of process principle and effects of various process parameters on the MRR. It has also been observed that very few theoretical/numerical studies have been reported for the prediction of MRR during Sinking–ECSM. Present work is an attempt in this direction. In this paper, an axisymmetric finite element transient thermal model has been developed to estimate the temperature field due to Gaussian distributed input heat flux of single spark. The estimated temperature field is further post processed for calculation of MRR during Sinking–ECSM. Particular attention has been paid to study the effects of energy partition, duty factor, spark radius, and electrolyte concentration on MRR during Sinking–ECSM of silicon nitride workpiece.

II. Modeling for Temperature Field within the Heat Affected Zone of Single Spark

The configuration of a Sinking–ECSM setup is shown in Fig.1. In ECSM the hydrogen gas bubbles are formed at the tip of the tool electrode. The coalescence of bubbles forms a gas film around the tip of the tool electrode when the supply voltage reaches a critical value. This gas film isolates the tool electrode from the electrolyte. Electrical discharges in the form of sparks take place in this gas film and machining of material is possible if the workpiece material is kept in the vicinity of the sparking zone. The material removal in Sinking–ECSM is mainly caused by the melting and vaporization due to heat generated by the spark. For the modeling of temperature field in the heat affected zone of single spark, following simplifying assumptions are made:

i) Workpiece material is homogeneous and isotropic.
ii) Only a fraction of total spark energy of a single spark is dissipated as heat into the workpiece. Remaining heat is assumed to be distributed between the tool and the electrolyte.
iii) At a time only one spark is produced at the workpiece top surface and the duration of spark is same for all sparks. The zone of influence due to single spark is assumed to be axisymmetric in nature $\left(\frac{\partial T}{\partial \theta}=0\right)$.
iv) The boundaries (B_2 and B_3) of the domain (Fig. 2), away from the heat flux are chosen at such a distance that there is no heat transfer across those boundaries i.e. $\frac{\partial T}{\partial n}=0$.
v) Shape of heat flux is assumed to be *Gaussian* distributed. From the experimental studies of Kulkarni et al. (2002) for single spark, the crater shape was observed as dome shape (part of sphere). So reflecting the shape of crater, the nature of the heat flux can safely be approximated as *Gaussian*.
vi) Ejection efficiency is assumed to be 100%. Also, there is no deposition of recast layer on the machined surface.

III. MATHEMATICAL FORMULATION

The governing heat conduction equation within the workpiece domain (Fig. 2) is given by:

$$\rho C_p \frac{\partial T}{\partial t}=\frac{1}{r}\frac{\partial}{\partial r}\left(k\, r\frac{\partial T}{\partial r}\right)+\frac{\partial}{\partial z}\left(k\frac{\partial T}{\partial z}\right) \qquad \text{in domain ABCD (Fig. 2)} \qquad (1)$$

Where, T is temperature, ρ is density, C_p is specific heat, and k is thermal conductivity of the workpiece material. In the above equation thermal conductivity and specific heat of work piece material are taken to be temperature dependent.

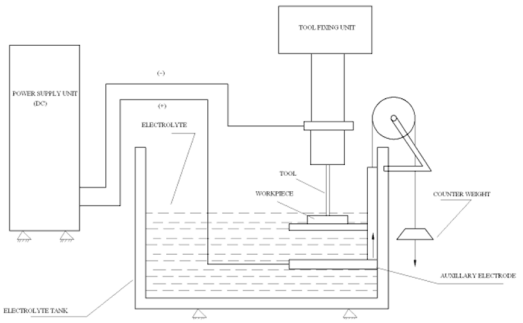

Fig.1 Configuration of DS–ECSM set-up

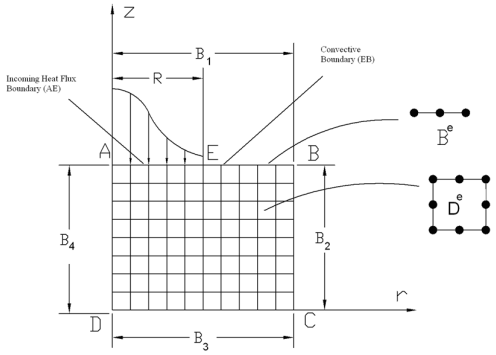

Fig. 2 Computational Domain with boundary conditions for Sinking–ECSM process

The initial condition for temperature of the entire domain at the start of machining is considered to be room temperature, T_0.

When $t=0$, $T(r,z)=T_0$ in domain ABCD (Fig. 2) (2)

The boundary conditions of the heat affected zone (Fig. 2) owing to single spark are as follows. On the top surface B_1, heat flux is considered only upto a radius equal to that of the spark radius (R). For the rest part of B_1, convective heat loss to electrolyte is considered. Further, the boundaries B_2 and B_3 are considered at such a large distance so that there is no heat transfer takes place across them. The boundary B_4 is an axis of symmetry. Thus the boundary conditions can be mathematically written as:
When t >0

$$-k\left(\frac{\partial T}{\partial z}\right)=\begin{cases} h(T-T_0) & if\ r>R \\ q_w(r) & if\ r\le R \\ 0 & for\ off-time \end{cases} \qquad on\ B_1 \tag{3}$$

$$\frac{\partial T}{\partial n}=0 \quad on\ B_2, B_3, B_4 \tag{4}$$

Here, $q_w(r)$ is the quantity of heat flux owing to the spark, h is the convective heat transfer coefficient, T_0 is the room temperature of electrolyte and n is outward normal to the boundary.

In the present work a Gaussian heat flux distribution is assumed and the expression for heat flux at any radius r, $q_w(r)$ to the workpiece is derived as:

$$q_w(r)=\frac{4.45F_wVI}{\pi R^2}\exp\left\{-4.5\left(\frac{r}{R}\right)^2\right\} \tag{5}$$

Where, R is spark radius, r is the radial distance from the axis of the spark, V is supply voltage, I is circuit current and F_w is energy partition.

The model proposed by Jain et al. (1999) for calculation of circuit current during Sinking–ECSM, is used in the present work:

$$I=0.1009V^{0.4815}k^{0.3420}\phi^{0.3420}d^{0.2881} \tag{6}$$

Where, k is electrolyte conductivity, ϕ is tool diameter and d is depth of the tool inside electrolyte. Dependence of the electrolyte conductivity on the concentration (C) of the NaOH electrolyte is given by (Jain et al., 1999):

$$k=0.885958+4.62384C-0.193274C^2-0.00208907C^3 \tag{7}$$

Based on literature for numerical calculation F_w during Sinking–ECSM. Earlier studies (Jain et al., 1999; Bhondwe et al., 2006) have used this value as 20%. Therefore in the present study F_w is taken as 20%.

For computational analysis of Sinking–ECSM process another important parameter required is the spark radius. However, quantification/measurement of the spark diameter is extremely difficult due to very high pulse frequencies. Basak and Ghosh (1997) have taken spark radius equal to 0.5×10^{-6} times circuit opening current in ampere for spark channel cylindrical in shape. Jain et al. (1999) assumed prismatic nature of spark with square cross section which is far from real life situation**.** Kulkarni et al. (2002) have given the crater diameter for different workpiece materials as 300μm based on their experiments. Therefore, in the present work, the spark radius is taken as 150μm.

In general, the material thermal properties such as specific heat capacity and thermal conductivity are temperature dependent. Earlier thermal models available in literature for Sinking–ECSM have assumed temperature independent thermal properties of the workpiece. In the present work, the temperature dependent thermal properties of silicon nitride workpiece are taken into account. The best fit curves are obtained to find the nature of variation in polynomial equation form, which are used in the numerical calculations. The polynomial equations are given below:

$$\begin{aligned} k &= 37.1558-0.0314T+1.26966\times10^{-5}T^2-9.242\times10^{-10}T^3-5.87147\times10^{-13}T^4 \\ C_p &= 413.21721+1.45487T-0.00121T^2+5.29355\times10^{-7}T^3-9.30496\times10^{-11}T^4 \end{aligned} \tag{8}$$

IV. Finite Element Formulation

The present analysis the Galerkin's weighted residual method [12] has been applied to obtain the temperature distribution within the computational domain (Fig.2) due to heat flux of single spark. The following elemental equations are obtained when Galerkin's approach is applied to Sinking–ECSM process (1-7).

$$[C]^e\left\{\dot{T}\right\}^e+[K]^e\{T\}^e+[K]^b\{T\}^b=\{f_C\}^b+\{f_q\}^b \qquad (9)$$

where,

$$\left.\begin{aligned}
[C]^e &= \int_{D^e} \rho C_p \{N\}^e \{N\}^{eT}\, dD^e \\
[K]^e &= \int_{D^e} k[B]^{eT}[B]^e\, dD^e \\
[K]^b &= \int_{B_h} h\{N\}^b \{N\}^{bT}\, dB_h \\
\{f_C\}^b &= \int_{B_h} T_0 h\{N\}^b\, dB_h \\
\{f_q\}^b &= \int_{B_q} \{N\}^b q_w\, dB_q
\end{aligned}\right\} \qquad (10)$$

The Gauss quadrature technique is used to evaluate elemental matrices and vectors. When elemental quantities of (10) are assembled, the following differential equations are obtained.

$$[GC]\left\{\dot{T}\right\}+[GK]\{T\}=\{GF\} \qquad (11)$$

Where, $[GC]$ is the global capacitance matrix, $[GK]$ is the global stiffness matrix, $\{GF\}$ is the global heat flux vector, $\{T\}$ is global temperature vector and $\left\{\dot{T}\right\}$ is time derivative of $\{T\}$. Equation (11) is converted into algebraic equations after application of implicit Finite Difference Method (FDM). Here, the solution marches in time, in steps of Δt until the desired final time is reached. In the present model, Δt is divided into two-time steps Δt_1 and Δt_2. Δt_1 and Δt_2 are pulse on time and off time of the spark, respectively

V. Modelling for Material Removal Rate

Formulation of section 2.2 is used for the development of an FEM based code using Matlab 7.0.1. The developed code calculates the temperature field in the workpiece due to Gaussian distributed input heat flux of a single spark. The material removed by a single spark can be calculated by assuming that the material having temperature more than the melting temperature is completely removed. Hence, melting isotherm is plotted using the result of temperature distribution in the zone of influence of single spark under the applied process conditions. The volume of the material removed by single spark is calculated as follows:

$$Vol = \int_{z_1}^{z_2} \pi r^2\, dz \qquad (14)$$

The volume obtained by Equation (14) is for single spark. The volume of material removed per unit time is calculated by:

$$MRR = Vol \times Sparking\ \ frequency = Vol \times \frac{1}{t_p} \qquad (15)$$

where, t_p is pulse time.

VI. Results and Discussions

Sarkar et al. (2006) have experimentally measured MRR from silicon nitride workpiece of size 20 mm × 20mm ×5mm during DS–ECSM. In their experiment a stainless steel tool electrode with a diameter of 400 μm was used as cathode. NaOH electrolyte with 10 to 30 wt. % electrolyte concentration was used. The workpiece was clamped just below the tool tip, and the tool tip was immersed 2-3 mm below the upper level

of the electrolyte. Experiments were carried out at five different voltage levels: 50 V, 54 V, 60 V, 66 V, and 70 V using pulsed DC power supply.

The above-mentioned problem is solved using present model for determination of MRR from silicon nitride workpiece during DS–ECSM. The wokpiece material and machining conditions used are taken same as used in the literature (Sarkar et al., 2006). The material properties of silicon nitride are taken from Guyer and Brownell (1989). Because of computational limitations of our computing system the domain size has been changed from 20 mm × 20mm ×5mm to 600 μm × 600 μm × 600 μm and since, the 3-D problem is approximated to a 2-D problem the workpiece domain is discretized into eight noded quadrilateral elements (Fig. 2). Convergence test was carried out by increasing the number of elements in the mesh. The simulation showed that the nodal temperature of workpiece domain obtained were essentially unchanged, when the mesh size is in excess of 1024 elements. The mesh of 1024 elements is thus found to be adequate for convergence. Hence the mesh consisting of 1024 number of elements with total 3201 nodes are used for further calculations. The nodal temperature in the workpiece domain is found using computer with Pentium 4 processor.

MRR is calculated for different supply voltage. MRR calculated using present FEM based model is compared with experimental values obtained by Sarkar et al. (2006). The results obtained using present model show) similar pattern as given in literature (Sarkar et al., 2006). MRR calculated using present FEM based model increases with increase in supply voltage. Calculated MRR at supply voltage of 50V using present FEM based model is found as $0.0032mm^3$/min whereas the experimental value of MRR for the same input condition is $0.0025mm^3$/min. Further, when the supply voltage increases to 60V the MRR calculated using present FEM based model is found as $0.0062mm^3$/min, whereas experimental value is $0.0041mm^3$/min. At the supply voltage of 70 V the calculated MRR is found $0.0096mm^3$/min against experimental MRR of $0.0083mm^3$/min.

The calculated MRR using present model is higher than the experimental MRR for each value of the supply voltage. This may be due to the value considered for ejection efficiency in present model during DS–ECSM process. In the present model the ejection efficiency is assumed to be 100% (it is assumed that all the material, which is melted, is removed). In real situation, some part of the molten material is not completely removed but it adheres back (resolidify) to the parent material because of the quenching effect caused by liquid electrolyte. This plays a dominant role, as the ejection efficiency in DS–ECSM is very low. It may be as low as 10% or even lower than that (Jain et al., 1999). Further there is no exact data available regarding energy partition and spark radius for the combination of silicon nitride workpiece, NaOH electrolyte and stainless steel tool electrode. Above described reasons are responsible for getting different values of computational and experimental results.

VII. PARAMETRIC STUDIES

The influences of process parameters such as energy partition, duty factor, spark radius and electrolyte concentration on MRR and ASR during DS–ECSM have been studied. Silicon nitride is taken as workpiece material. Governing equation, Initial and Boundary conditions as discussed in section 2.1 are taken same through out the parametric studies.

A. Effect of energy partition

The effect of energy partition (F_w) on MRR during DS–ECSM is studied. Here it is observed that MRR increases with the increase in energy partition. 606% increase in MRR is observed by increasing the energy partition by 10%. Increase in the energy partition means the amount of heat going to the workpiece is more, which is responsible for larger volume of material melting and hence high MRR.

B. Effect of duty factor

Duty factor is the ratio of spark on-time and pulse duration (on-time + off-time). Duty factor has been taken by considering off-time 500μs and varying the on-time. The effect of duty factor on MRR in DS–ECSM is studied. Here it is observed that MRR increases with the increase in duty factor. 145% increase in MRR is observed by increasing the duty factor by 13%. With increase in duty factor, the spark energy will be transferred to the workpiece for more time because of which volume of workpiece material melted is also more. Hence, the MRR is increased with increase in duty factor.

C. Effect of spark radius

The effect of spark radius on MRR is studied. Here it is observed that MRR is decreasing from $0.0165mm^3$/min to $0.0021mm^3$/min if spark radius is changed from 130µm to 160µm. This shows a decreasing trend of MRR with respect to increase in spark radius. This is because, heat flux decreases with increase in spark radius. Due to lower heat flux less volume of material is melted and hence MRR decreases with increase in spark radius.

D. Effect of electrolyte concentration

The effect of electrolyte concentration on MRR is also studied.The MRR goes on increasing from 6% electrolyte concentration to 10% electrolyte concentration and then starts decreasing. This is due to the fact that the specific conductance of NaOH solution increases up to 10%, beyond which it starts decreasing (Jain et al., 1999). An increase in specific conductance means increased electrolyte conductivity and consequently more circuit current. An increase in circuit current would mean the accelerated electrolysis process. It would result in greater rate of evolution of hydrogen bubbles at the cathode. The increased rate of formation of gas bubbles at the cathode implies an enhanced rate of sparking and hence higher MRR. When the concentration is increased beyond 10%, rate of electrolysis decreases. Due to increased rate of reactions, mobility of the ions is decreased and in turn the specific conductance of the electrolyte is decreased. Therefore, beyond a certain value of electrolyte concentration (C=10%), change in the circuit current decreases. Since, the heat energy developed from the spark is proportional to the circuit current, the material removed will be less at higher values of concentration.

VIII. CONCLUSIONS

In the present work, an axisymmetric FEM based transient thermal model has been developed for the determination of MRR during Sinking–ECSM. The present model is used to study the influence of different input parameters such as energy partition, duty factor, spark radius and electrolyte concentration on MRR during Sinking–ECSM of silicon nitride workpiece material. Following conclusions have been derived from the present analysis.

1. The trend of variation of computed MRR with supply voltage has been found similar to that observed experimentally. The computed MRR values are found higher than those obtained experimentally because of 100% ejection efficiency consideration.
2. With increase in energy partition (F_w), there is increase in MRR. Improvement in MRR by 606% have been found by increasing F_w by 10%.
3. Increase in MRR has been found with increase in duty factor. A 145% increase in MRR is observed by increasing duty factor by 13%.
4. MRR decreases with increase in spark radius during Sinking–ECSM. Here it is observed that 23% increase in R decreases MRR by 87%.
5. MRR is found to increase with increase in NaOH electrolyte concentration up to 10% but it starts to decrease if concentration is further increased.

REFERENCES

[1] E. C. Guyer, and D. L Brownell, Hand Book of Applied Thermal Design, McGraw-Hill Book Company, New York, 1989.

[2] A. Kulkarni, R. Sharan and G. K. Lal, An experimental study of discharge mechanism in electrochemical discharge machining, International Journal of Machine Tools and Manufacture. 42 (2002) 1121-1127.

[3] J.N. Reddy, An Introduction to Finite Element Method, third ed., Tata McGraw-Hill Publishing Company Limited, New Delhi, 2005.

[4] S. S. Rao, The Finite Element Method in Engineering, fourth ed., Elsevier Publication, New Delhi, 2005.

[5] K. L. Bhondwe, V. Yadava and G. Kathiresan, Finite element prediction of material removal rate due to electrochemical spark machining, International Journal of Machine Tools and Manufacture. 46 (2006) 1699-1706

[6] S. N. Joshi and S. S Pande., Development of an intelligent process model for EDM, International Journal of Advanced Manufacturing Technology, (2009) DOI: 10.1007/s00170-009-1972-4.